Nitrogen atom energy distributions in a hollow-cathode planar sputtering magnetron

Zhehui Wang[a], Samuel A. Cohen, D. N. Ruzic[b], and M. J. Goeckner[c]

Plasma Physics Laboratory, Princeton University,

P.O. Box 451, Princeton, NJ 08543

May 31, 1999

Abstract

Energy distributions of N atoms in a hollow-cathode planar sputtering magnetron were obtained by use of optical emission spectroscopy. A characteristic line, N I 8216.3 Å, well-separated from molecular nitrogen emission bands, was identified. Jansson's nonlinear spectral deconvolution method, refined by minimization of χ_w^2, was used to obtain the optimal deconvolved spectra. These showed nitrogen atom energies from 1 eV to beyond 500 eV. Based on comparisons with VFTRIM results, we propose that the energetic N atoms are generated from N_2^+ ions after these ions are accelerated through the sheath and dissociatively reflect from the cathode.

PACS numbers: 51.50.+v, 52.50.Dg, 52.75.Rx

I. Introduction

Neutralization is likely when an ion backscatters from a metal surface. Many experiments have studied backscattering for ion energies above a few hundred eV. At somewhat lower impact energies, 5 - 100 eV, Cutherbertson *et. al* [1] measured reflected-

[a] email: zwang@lanl.gov Current address: Los Alamos National Laboratory, MS E526, Los Alamos, NM 87544

[b] Department of Nuclear Engineering, University of Illinois

[c] Varian Associates, Inc.

atom energy distributions for atomic ions backscattering as neutrals. Knowledge of reflected-atom energy distributions in the range 1-500 eV is essential for understanding basic ion-surface interactions, thin-film deposition processes, plasma-dust interactions, and Langmuir-probe operation.

Molecular ion species bombardment of surfaces is a more complex phenomena, important in many atmospheric plasmas, e.g., space craft reentry, and many laboratory plasmas, e.g., the deposition of TiN or Al_2O_3 compound films. Computational methods,[2] widely used to model the reflected-atom energy distribution for atomic bombardment, have been less commonly applied to molecule backscattering because of the increased complexity and lack of experimental data to compare with the models.

In many laboratory plasmas, the electron temperature is only few eV and the ionization fraction less than 1%. Under such conditions, bi-atomic molecule (H_2, N_2, *etc*.) discharges usually contain both atomic (H^+, N^+) and molecular ions (H_2^+, N_2^+). Both types of ions contribute to the reflected *atom* flux, the latter *via* fragmentation upon impact. This manuscript reports on the atomic-N energy distribution in a hollow-cathode planar sputtering magnetron (HCPM).[3] In this paper we argue that the energetic N atoms observed are due to dissociative reflection of molecular ions which impact the cathode.

Nitrogen-atom energy distributions were obtained using optical emission spectroscopy (OES) wherein plasma electrons excite atomic and molecular species which then spontaneously decay, emitting visible-wavelength photons. OES has been used to characterize the species in plasma, to measure electron density, electron temperature T_e [4] and electron energy distribution function (EEDF), and ion and atom densities[5] and temperatures. Here we report on its application to the measurement of atomic-N energy distribution in a sputtering magnetron.

The ability to observe weak emission from backscattered nitrogen atoms arises from the fact that, in a molecular nitrogen discharge, the background light is due primarily to

molecular nitrogen. Therefore, the background light near atomic N lines *may* be greatly reduced and we *may* then be able to see a relatively weak signal due to the backscattered N atoms. Finding a spectral region where molecular emission is weak is actually quite a task.

In this paper we also describe the effects on the spectra of operational parameters, such as cathode material, bias voltage and gas pressures, and also the heating of the ambient gas by backscattered atoms. The experimental data are compared with a numerical model (VFTRIM[6]) of backscattering. Based on this study, the mechanism for generating energetic atomic N in a molecular nitrogen discharge is proposed.

II. Experiment

Experiments were carried out on a hollow-cathode planar sputtering magnetron (HCPM), see Figure 1. Details of the operation of a HCPM can be found in previous papers. [3, 7] A negative DC bias (300-1500 V) is placed on the cathode structure. Ions impact there, ejecting secondary electrons which are accelerated through the cathode sheath. Within the plasma these electrons cause ionization events, replenishing the loss of ions to the cathode.[8] In brief, the HCPM acts much like a classical glow discharge, but with more efficient use of the energy of the ejected electrons because of the hollow cathode geometry and the magnetic field.

A schematic of the light detection setup is shown in Fig. 2. An Acton research SP500 spectrometer (0.5-meter focal length, Czerny - Turner type) with 1200 g/mm grating was used. The detector was a Hamamatsu R636 – 10 photo-multiplier tube (PMT), which has high quantum efficiency in the region of interest, near 8000 Å. Cooling of the PMT was necessary to reduce its dark current a factor of 100, thereby increasing the signal-to-noise ratio. When obtaining a high-resolution line profile, the spectrometer was scanned at a rate of 1 Å /min., to provide long exposure.

Using ~~a~~ the 826.45 nm line emitted from an argon Geissler tube, the instrumental width of the spectrometer was measured to be 0.07 nm. (The measured line showed a

Gaussian shape.) This corresponds to an instrumental temperature of 17.1 eV for nitrogen. (The same line had a width of 0.02 nm when measured with a Fabry-Perot spectrometer.) We note that the primary mechanism for line broadening in the HCPM is the Doppler effect. The Zeeman and Stark effects are relatively unimportant at the low magnetic field and plasma density of these experiments.[9]

Post-processing of PMT signals was done in several steps: 1.) Pre-amplification and conversion of current signals to voltage signals. 2.) Integration of the voltage signals. 3.) Digitization of the analog voltage signals. 4.) Storage of the digitized signals in a memory module. The spectrometer grating, data acquisition and processing system were properly timed by a Power Mac 7100 using LabVIEW.

III. Results

The spectra can be analyzed in two steps. First one can look at the spectra as a whole, i.e., the area under the spectra line, to examine the population of N atoms. This includes both thermal atoms and hyperthermal atoms. Because, as will be shown below, the thermal population is significantly larger than the hyperthermal population, the spectral line area can be used as a measure of the thermal population. In the second step, the detailed shape of the spectra will be analyzed to look at the fraction of the spectra (< 1%) that corresponds to the hyperthermal component.

Correspondingly, there are two parts to this Section. Part A presents results that are obtained in a straightforward analysis of the raw data. It first presents the overall spectrum from the plasma and the identification of a suitable N I line. It then describes the dependence of the peak emission on plasma current and finally a temperature to characterize the cool, *ca.* < 10 eV N atoms. That energy could arise from Franck-Condon dissociation of nitrogen molecules or be part of the slowing-down spectrum of faster neutrals created by backscattering of energetic ions. Part B presents analyzed data, obtained *via* a very powerful deconvolution method described in much detail in the references.[10, 11] This

refinement allows determination of the N atom velocities, rather than simply a temperature. In part B we also extend the analysis to larger Doppler shifts, hence to more energetic particles.

A. Bulk atom emission intensity and temperature

Figures 3 and 4 show the observed spectrum (670-970 nm and 370-670 nm) for a N_2 HCPM plasma with 190 mA cathode current and 407 volt cathode bias. Of the ~40 spectral lines labeled, only one (group), at 821.6 nm, is due to atomic N. The others are primarily due to N_2 . A few lines attributable to sputtered copper are also visible. (For an H_2 plasma, a spectral scan with identical sensitivity and resolution over the same wavelength region did not reveal any bright atomic lines sufficiently separated from molecular emission to allow a useful study.) A higher resolution spectral scan of the N_2 plasma is shown in Figure 5 for the spectral region 810 - 830 nm. All these lines are due to N I.[12] The 821.6 nm line, due to the transition 3p ^{4}P -> 3s ^{4}P (J'=5/2 -> J = 5/2) is chosen for most analysis since it is the brightest. Note that the nearest lines are +6.8 Å and -5.6 Å away. Energy-wise, these lines would corresponds to Doppler-shift for N atoms of about 4 keV, which is well beyond the experimental cathode bias of up to 1500 V. Hence these neighboring N lines do not contaminate the spectra we obtained.

Following Rossnagel and Saenger[13] or Gau and Lieberman,[14] the intensity of the N I 8216.3 Å as a function of total cathode current was measured, Fig. 6. This is to elucidate the source of the nitrogen atoms responsible for the peak of the emission from the N I 8216.3 Å line. (Intensity here means the line's peak value.) Data shown are for different N_2 pressures $p(N_2)$ ranging from a few mTorr to about 100 mTorr. From the fitting shown, we see that the emission intensity $\mathcal{I}$ is proportional to background pressure $p(N_2)$ and cathode current J to the first power. The peak intensity includes only a small contribution from energetic neutral particles because of their large Doppler-shift.

$$\checkmark = p(N_2) \times J. \quad (1)$$

Figure 7 shows Doppler broadening of the 8216.3 Å line at different pressures, in comparison with the instrumental profile. A blue-red asymmetry is seen. Accordingly, we define two temperatures, a blue-shifted and a red-shifted, each represented by a half-Gaussian. The (blue or red) bulk N temperature T_o was obtained by subtracting the raw data temperature T_s which is proportional to (the square of) the full width at half-maximum (FWHM) from the instrumental T_I:

$$T_o = T_s - T_I \quad (2)$$

As a function of discharge pressure, the blue and red bulk N temperatures are shown in Fig. 8. The asymmetry is clear, with the blue-shifted (forward-moving) N atoms being warmer than the red-shifted. The bulk temperatures increase with pressure.

Fig. 8 shows bulk N atom temperatures in the range 1-15 eV, increasing as the pressure is increased. The temperature on the blue-shift side is always greater than on the red-shift side. The magnitude of the temperature is understandable in a qualitative fashion. The formation of neutral N atoms with these low energies proceeds primarily by Franck-Condon dissociation of N_2. The energy of Franck-Condon neutrals depends on electron energy. For example, at low electron energies, *ca.* 20 eV, the main process is *via* excitation from the $X\ ^1\Sigma_g$ state to the auto-dissociating $C'\ ^3\Pi_u$ state, creating N atoms in the range 1.4 - 4.4 eV.[15] Higher energy electrons can promote excitation to auto-dissociating states which produce more energetic electrons, to ~ 10 eV. Randomization of the Franck-Condon energy produces a temperature approximately 1/2 of the energy, consistent with the low pressure data of Fig. 8. The asymmetry of the temperatures may be due to collisions with sputtered atoms or backscattered impacting ions.

B. N atom energy distribution

With high-*Z* (tungsten, W) and low-*Z* (aluminum, Al) targets, the spectra near the N I 8216 Å line were obtained along a view that is perpendicular to the surface of the target, as shown in Fig. 1. High and low gas pressures were studied, Fig. 9 to Fig. 12. The following discussion is based on the deconvolved data, the solid line in each figure. The deconvolution technique is described elsewhere in more detail.[10, 11]

Fig. 9 is obtained for a 279 mA HCPM discharge, with cathode bias = -1114 V, above a W target at a N_2 pressure of 2.74 mTorr. (A pressure less than five mTorr is in the low-pressure regime defined[3] in our earlier experiments.) The peak intensity at N I 8216 Å is over a 100 times stronger than a few Å away. The peak of the emission line profile (labeled as background emission in the Fig. 7) is due to the cool N atoms just discussed, those with up to a few eV in energy, and with a Doppler shift ≤ 0.4 Å.

The 1σ level (straight dashed line in the figure) is the noise level, defined as the average signal level (of the smoothed curve) towards the outer wings (left and right) of the line peak. The noise level is determined by sum of the electronics noise, amplifier noise, digitizer noise, background light emission, *etc*. Signals at twice the noise level, 2σ level (solid straight line in the Fig. 7) have about an 80% statistical likelihood to be due to N-atom emission.

The deconvolved signal exceeds the 2 σ level from the peak out to a relative wavelength of about -2 Å in the blue-shift direction and to + 1.6 Å in the red-shift direction. The peak at a -2.2 Å shift in wavelength would arise from N atoms having an energy of about 475 eV. These are the most energetic N atoms, according to the spectral line profile, and are labeled as such in Fig. 9. The region between -1.8 Å and the peak is labeled in Fig. 9 as the *slowing-down structure*. The slowing-down structure will be discussed in more detail later. A small but interesting feature, labeled as 8217.9 Å, is

noted. Its interpretation as a spectral line is discussed after consideration of spectra obtained with an Al cathode.

Fig. 10 is a data set for an Al cathode at low pressure, 4.38 mTorr. Besides lower *Z* value compared with W cathode case, the cathode bias of the HCPM, -369 Volts, is much smaller than the -1114 Volt bias used for the W cathode. Similar to Fig. 9, the background emission due to cold N atoms is about 100 times more intense than the rest. Compared with Fig. 9, we see above the 2σ level only three sharp spectral structures, but no extended slowing-down structure. The power of Jannson's deconvolution method is clear as it reveals sharp spectral features at 8217.9 ± 0.1 Å and 8215.0 Å. The wavelengths of the deconvolved lines shown are not affected by choice of the deconvolution parameters. The 8217.9 Å feature appeared in Fig. 9, just above the $2\ \sigma$ level. Furthermore, its existence and location were found to be independent of cathode bias. Therefore, we identify it as a spectral line instead of relating it to Doppler-shifted N I 8216 Å. More discussion on the dependence of energy spectra on cathode bias is given later. This line at 8217.9 Å may be a nitrogen line, because its existence does not depend on target material. However, we have not found a nitrogen atom or ion line at this wavelength listed in the standard spectral tables. The origin of the other sharp spectral feature, at 8215.0 Å, is also not clear and deserves further investigation. These two spectral features are not due to sputtered W atoms, according to the spectral line tables.[12]

For the Al cathode, the deconvolved spectrum in Fig. 10 shows very little light between -0.2 and -1.2 Å.

Fig. 11 is for a W cathode at higher gas pressure, 34.5 mTorr, and lower cathode bias, -570 Volts. Again, a slowing-down structure is identified, but extends to only -1.8 Å. For N atoms, this Doppler shift corresponds to 316 eV. Again the long tail at the red-shift side is seen. The red-shifted long tail and the blue-shifted slowing-down structure can be fit

by a shifted-Maxwellian distribution with temperature on the order of 50 eV. Again, the spectral line 8217.9 Å shows up.

The deconvolved spectrum in Fig. 12, for the Al target, also at higher pressure (30.4 mTorr) and lower voltage (339 V) shows simple structure. Only emission near the peak is above the 2σ level.

In the following discussion section we convert the spectra into energy distributions and compare them with a numerical model of scattering, VFTRIM.

IV. Discussion

From energy considerations, the mechanism for generating energetic neutral atoms (with more than 50 eV) in the HCPM must be related to ions colliding with the cathode surface. Ions are produced in the plasma by electron impact and have initial energy V_0 less than a few eV. Futhermore, only a small electric field exists within the plasma. It is when ions fall through the cathode sheath, in the absence of collisions , that they gain appreciable energy, equal to the full cathode bias V_b. Therefore the upper limit energy E_i when these ions strike the cathode surface is

$$E_i = V_b + V_0 \sim V_b \,. \tag{3}$$

An energetic ion can be reflected as a neutral particle, retaining a substantial fraction of its incidental energy. The energy retained depends on ion species, the cathode material, lattice structure, incidental angle, incident ion energy, as well as number of collisions this ion experiences as it transverses the plasma.

For plasma discharges involving molecular gases, such as N_2, the ions involved can be atomic ions N^+, or molecular ion N_2^+. We can conceive of three distinct sequences by which energetic atomic neutrals may be produced.

1.) From N^+ ions. A N^+ hits the cathode surface, reflected as an energetic nitrogen atom N_E.

2.) From N^+ ions. A N^+ hits the cathode surface, reflected as energetic N_E^-. The N_E^- undergoes a second acceleration through the sheath, N_E^- charge-exchanges with an cold N, becomes a N_E: $N_E^- + N \rightarrow N_E + N^-$.

3.) From N_2^+ ions. A N_2^+ strikes the cathode surface, undergoes dissociative neutralization, and is reflected as two N_E s: $N_2^+ + e_s \rightarrow 2\ N_E$. ($e_s$ means an electron from the surface.)

We propose the third process as the main process for energetic N atom generation in our experimental conditions. The reasons are the following:

The energy to break the bond between the two Ns in a N_2^+ is around 9 eV. According to Winter and Horne,[16] the probability of a N_2^+ dissociating into 2 N atoms depends on the incident N_2^+'s energy when it is reflected from a metallic surface. For energies greater than 100 eV (much greater than the bond energy of 9 eV), the dissociation probability reaches unity for W, Ni, Mo targets. Our experimental conditions guarantee that all N_2^+s hit the cathode surface have energy above 100 eV. All the N_2^+s dissociate as two N atoms when they are reflected by cathode.

The reflection energy peak as function of cathode bias at low pressures, Fig. 15, showed that the maximum energy carried by energetic atoms is less than 50% of the total incidental energy of the ion (that is, the cathode bias). This is consistent with the proposition that the total incidental energy of any N_2^+ ion is equally distributed between two energetic N atoms generated in the dissociation process.

Finally, as suggested by the full visible range plasma emission spectra analysis, the largest fraction of ions in the discharges is N_2^+ under our experimental conditions. The N^+ ions are far fewer than N_2^+ within the discharge. Even N^+ ions do produce energetic N atoms, their signal is probably too small to be measured by the detector used.

The cause for the red-blue asymmetry is speculated to be the interaction between the Franck-Condon neutrals and the backscattered energetic N atoms. (The sputtered cathode

atoms may play a small role.) As shown in Figure 13, in a HCPM, plasma bombards the HCS side walls, as well as the planar region. At a pressure of 1 mTorr, the mean-free-path for energetic N atoms backscattered from the cathode is about 10 cm. Hence, even at the lowest pressures of our experiments, collisions between backscattered N and the Franck-Condon N population will transfer momentum to the Franck-Condon neutrals. Because the majority (70-90%) of the ions hit the planar cathode, the Franck-Condon distribution will preferentially drift towards the optics, creating a blue shift in their emitted light.

Two effects can contribute to the red shift. First, 10-30% of the ions hit the hollow cathode structure. When these backscatter they can provide momentum either towards or away from the optics. Secondly, the proximity of the walls allows collisions of the Franck-Condon neutrals with them. This will redistribute some of the energy into the red shifted direction.

Based on Fig. 9, 10, 11, and 12, energetic N arise from reflection from the W cathode. We have studied the energy distribution of N with W target at various pressures. In Fig 14 and 15, the Doppler shift of the N I 8216 Å line has been converted into energy unit (eV), i.e., as an energy distribution.

Compare N energy distribution for two pressures: p = 2.29 mTorr (Fig. 14) and p = 56.7 mTorr (Fig. 15). The most energetic N atoms for p = 2.29 mTorr have energies around 600 eV in Fig. 14. While the most energetic N atoms for p = 56.7 mTorr have energies about 300 eV in Fig. 15. Such difference is correlated with the different cathode biases, V = -1281 volts in Fig. 14 and V = -554 volts in Fig. 15. The VFTRIM results will support this connection.

There are two possible causes for a slowing-down structure. i.) The most energetic particles going side ways with respect to the sight of observation (These are *pseudo*-slowing-down particles because only the velocity component along the line of sight of observation were detected); ii.) Particles with less energy. (These are the *real* slowing-

down particles). From the mean-free-path considerations, even at low pressures collisions are important because of the HCS.

One way to discriminate between these two causes of the slowing-down structure is to look at the bulk particle temperature, determined by the width of the line peak. The bulk particle temperature is higher at higher pressure. Indicating that true slowing-down is occurring.

We now compare the measured maximum reflected N energy with VFTRIM simulations.

Fig. 17 shows VFTRIM typical simulation results for N collision with W (1200 V bias) and Al cathode (400 V bias) respectively. For Al cathode, reflected Ns retain up to 16% of the incident energy. For W cathodes, Ns retain about 40% of the total incidental energy. For an Al cathode bias of about 400 volts (similar to the experimental conditions), VFTRIM predicts less than 70 eV for each reflected N atom. This VFTRIM prediction is consistent with the deconvolved data shown Fig. 10 and Fig. 12. VFTRIM predicts about 500 eV reflected N for 1200-volt W-cathode bias. The most energetic N observed was about 589 eV, Fig. 16. This difference is only partly explained by the experimental error bar, as shown later in Fig. 19.

One detailed comparison of VFTRIM results with experiment is shown for plasma shot # 1103 in Fig. 18. Fig. 19 summaries the maximum experimental reflected N energy (in fraction of the bias) for W cathode at different cathode bias. VFTRIM predicts a constant fraction for maximum reflected energy while the experiment shows an increasing fraction with energy. Similar trend was also observed by Cuthbertson et al. [1] for atom collision with metal surface. The observed reflection energy peaks are less than 50% of the total N_2^+ incidental energy onto the cathode. For comparison, the result using simple binary collision model (N - W atom collision) which predicts that the reflected energy (E_{ref}) and

the cathode bias (V_{bias}) ratio is determined by the W atom mass (M_W) and N atom mass (M_N):

$$\frac{E_{ref}}{V_{bias}} = \frac{1}{2}\frac{M_W - M_N}{M_W + M_N} = 43\%. \quad (4)$$

This prediction is more than that of VFTRIM (about 37%). It agrees with experiment in the high energy (> 1 kV) end. Which might be suggesting that for high energy N -W cathode collisions, binary collision mechanism is important.[1] Because the molecular bonding energy is small in comparison with cathode bias, a bi-atomic ion collision with cathode is similar to that of two atoms collision with cathode independently, and therefore the factor 1/2 on the right hand side of the Eq. (4).

As mentioned, the VFTRIM simulations do not include particle transport through the plasma and gas, which is particular important for p > 13 mTorr. A more powerful code which includes both ion-surface interaction and transport of particles within the plasma could be more useful in a comparison with the experimental data presented here.

Acknowledgment

We are grateful to Mr. B. Berlinger and Mr. T. Bennett for their technical help. This work is supported by U.S. D.o.E Contract No.DE-AC02-76-CHO-3073

Figure caption

Figure 1, Dimensions of HCPM configuration and detection line of sight.

Figure 2, A schematic of the optics setup for the N energy distribution measurement.

Figure 3, A nitrogen discharge spectrum from 380 nm to 670 nm.

Figure 4, A nitrogen discharge spectrum from 670 nm to 970 nm.

Figure 5, Nitrogen atomic lines around N I 821.6 nm.

Figure 6, Intensity of N I 8216 Å lines λ dependence on cathode current J.

Figure 7, Comparison of the raw data N I 821.6 nm profiles with instrumental profile. The blue and red asymmetry is observed.

Figure 8, Bulk N temperature as a function of pressure, the error bars shown are typical.

Figure 9, N I 8216 Å line profile for p = 2.74 mTorr, V=1114 volts and J =279 mA, W target.

Figure 10, N I 8216 Å line profile for p = 4.38 mTorr, V=369 volts and J =312 mA, Al target.

Figure 11, N I 8216 Å line profile for p = 34.5 mTorr, V=570 volts and J =295 mA, with W target.

Figure 12, N I 8216 Å line profile for p = 30.4 mTorr, V=339 volts and J=256 mA, with Al target.

Figure 13, Blue and red shift are due to the ion-collisions with the HCPM cathode at different locations.

Figure 14, N energy distribution for p = 2.29 mTorr, V=1281 volts and J=281 mA, W target.

Figure 15, N energy distribution for p = 56.7 mTorr, V=554 volts and J=299 mA, W target.

Figure 16, Example of reflected N energy peak as a function of cathode bias for p = 2.45 mTorr, V=1288 volts, J= 337 mA, and W target.

Figure 17, An example of the VFTRIM prediction of the reflected N energy distribution for W cathode (dashed curve) and Al cathode (solid curve).

Figure 18, Detailed comparison of experimental N energy distribution with VFTRIM prediction under similar conditions, W cathode.

Figure 19, Peak reflection energy (in fraction of total cathode bias) vs. the cathode bias for W target. VFTRIM results are plotted in dashed line. Experimental data agree with simulation within the error bar. Also shown in the binary model result (solid line), as explained in text.

[1] J. W. Cuthbertson, W. D. Langer, and R. W. Motley, Journal of Nuclear Materials **196-198**, 113 (1992)
[2] W. Eckstein, Computer simulation of Ion-solid Interations, Springer-Verlag, Berlin (1991)
[3] Z. Wang and S. A. Cohen, J. Vac. Sci. Technol. **A 17**, 77 (1999)
[4] K. S. Fancey, and A. Matthews, Vacuum **43**, 1013 (1991)
[5] F. Guimarães, J. B. Almeida and J. Bretagne, Pl. Sources Sci. Technol. **2**, 138 (1993)
[6] D. N. Ruzic, and H. K. Chiu, J. Nucl. Mater. **162 - 164**, 904 (1989)
[7] Z. Wang and S. A. Cohen, Phys. Plasmas **6**, 1655 (1999)
[8] J. L. Vossen, and W. Kern, ed. *Thin Film Processes*, Academic Press, New York (1978).
[9] M. J. Goeckner, J. Goree and T. E. Sheridan, J. Vac. Sci. Technol. **A 8**, 3920 (1990)
[10] P. A. Jansson, ed., Deconvolution of Images and Spectra, Academic Press (1997)
[11] Z. Wang, PH. D Thesis, Princeton University (1998)
[12] A.N. Zaidel, V.K. Prokof'ev, S.M. Raiskii, V.M. Slavyni, and E.Yu. Shreider, *Table of Spectral Lines*, IFI/Plenum Data Corp (1970).
[13] S. M. Rossnagel, and K. L. Saenger, J. Vac. Sci. Technol. **A 7**, 968 (1989)
[14] L. Gau and M. A. Lieberman, J. Vac. Sci. Technol. **A 6**, 2960 (1988)
[15] J.T. Fons, R.S. Schappe, and C.C. Lin, Phys. Rev. A 53 (1996) 2239.
[16] H. F. Winter, and D. E. Horne, Surf. Sci. **24**, 587 (1971)

Figures

FIG. 1.

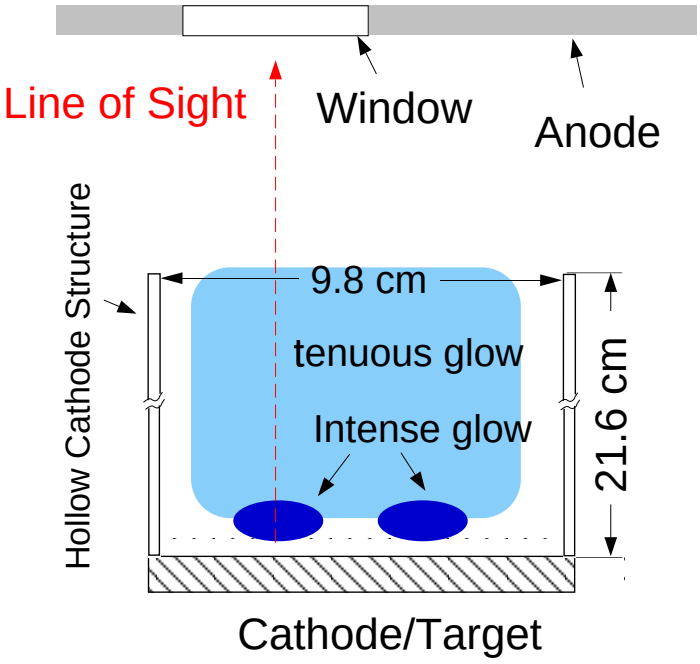

FIG. 2.

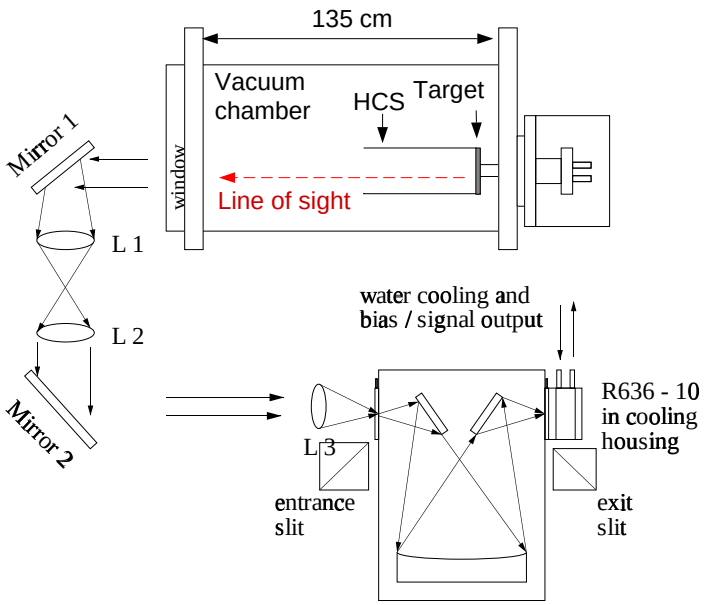

Acton Research SP 500

FIG. 3.

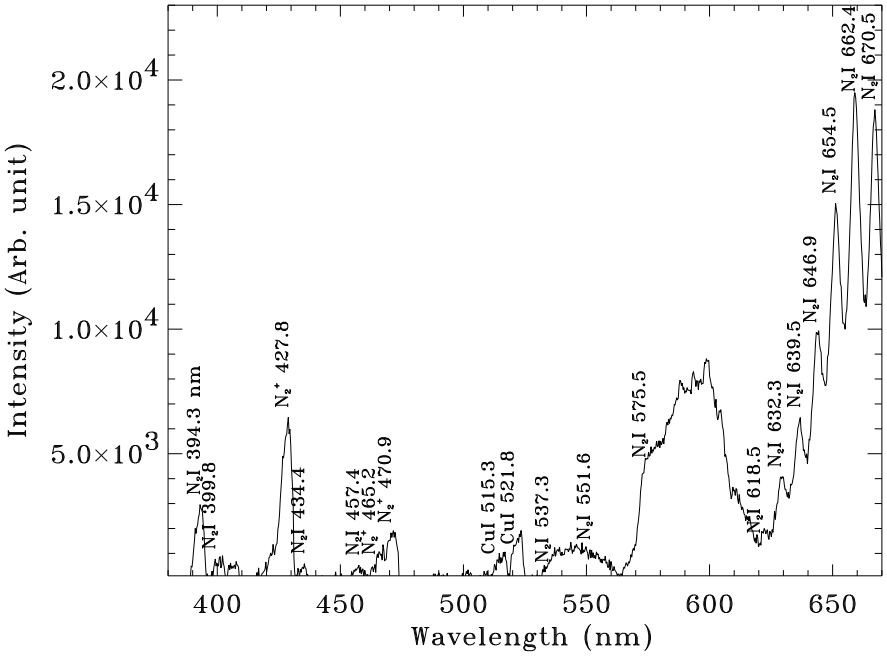
Intensity (Arb. unit)
2.0×10^4
1.5×10^4
1.0×10^4
5.0×10^3
400
450
500
550
600
650
Wavelength (nm)
N2I 394.3 nm
N2I 399.8
N2+ 427.8
N2I 434.4
N2I 457.4
N2I 465.2
N2+ 470.9
CuI 515.3
CuI 521.8
N2I 537.3
N2I 551.6
N2I 575.5
N2I 618.5
N2I 632.3
N2I 639.5
N2I 646.9
N2I 654.5
N2I 662.4
N2I 670.5

FIG. 4.

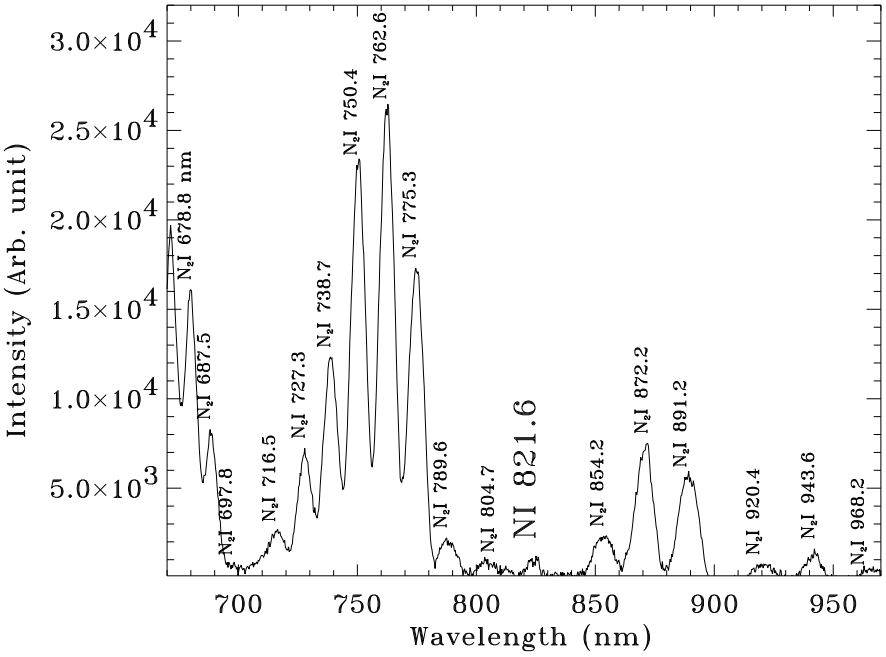
Intensity (Arb. unit)
3.0×10^4
2.5×10^4
2.0×10^4
1.5×10^4
1.0×10^4
5.0×10^3
700
750
800
850
900
950
Wavelength (nm)
N2I 678.8 nm
N2I 687.5
N2I 697.8
N2I 716.5
N2I 727.3
N2I 738.7
N2I 750.4
N2I 762.6
N2I 775.3
N2I 789.6
N2I 804.7
NI 821.6
N2I 854.2
N2I 872.2
N2I 891.2
N2I 920.4
N2I 943.6
N2I 968.2

FIG. 5.

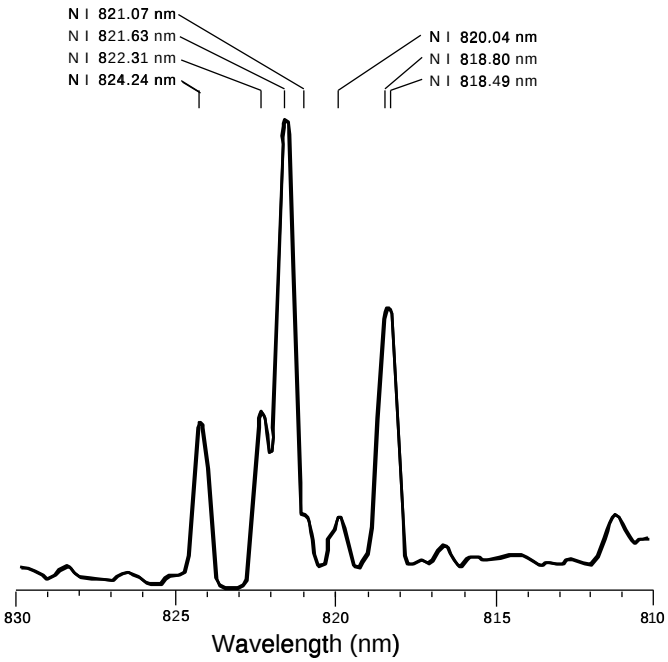
N I 821.07 nm
N I 821.63 nm
N I 822.31 nm
N I 824.24 nm
N I 820.04 nm
N I 818.80 nm
N I 818.49 nm
830
825
820
815
810
Wavelength (nm)

FIG. 6.

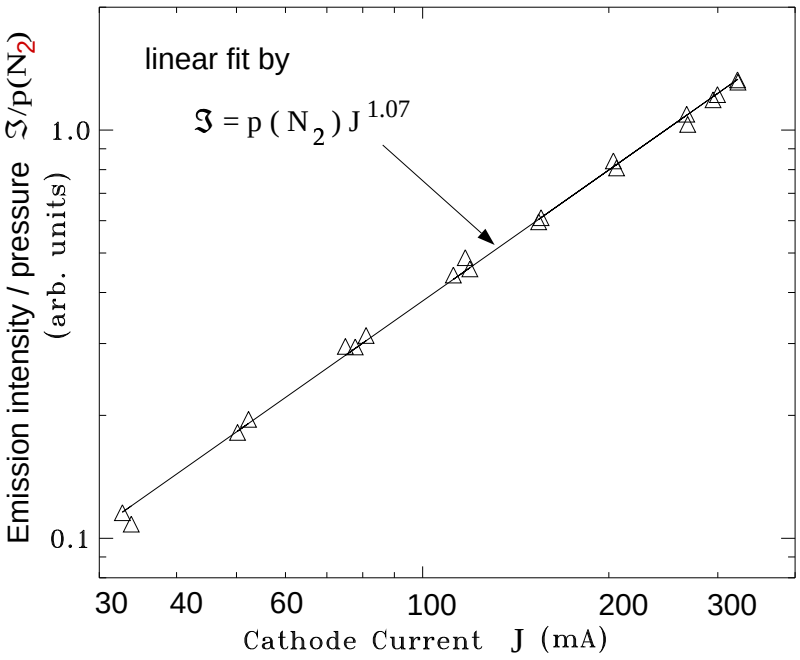
linear fit by
$\Im = p(N_2) J^{1.07}$
Emission intensity / pressure $\Im/p(N_2)$
(arb. units)
1.0
0.1
30
40
60
100
200
300
Cathode Current J (mA)

FIG. 7.

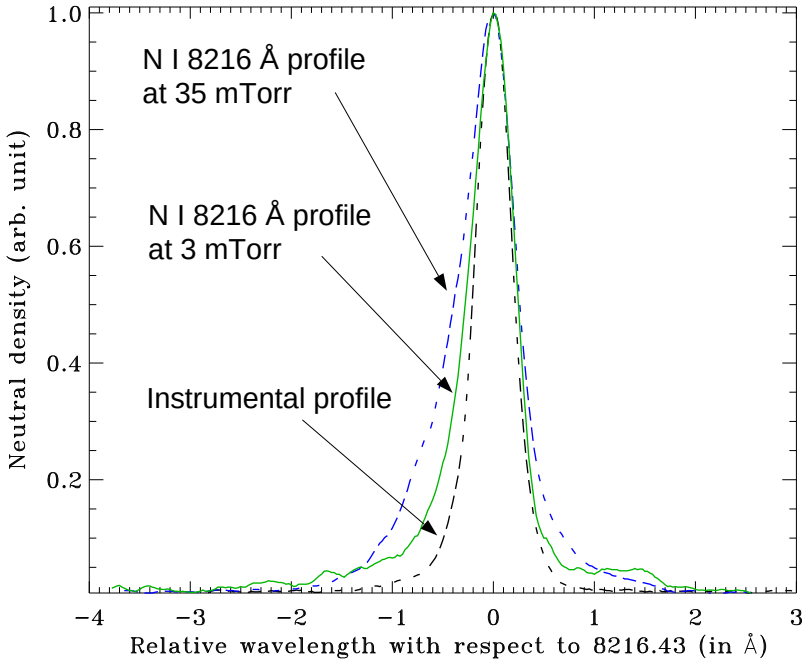
N I 8216 Å profile
at 35 mTorr
N I 8216 Å profile
at 3 mTorr
Instrumental profile
Neutral density (arb. unit)
1.0
0.8
0.6
0.4
0.2
−4
−3
−2
−1
0
1
2
3
Relative wavelength with respect to 8216.43 (in Å)

FIG. 8.

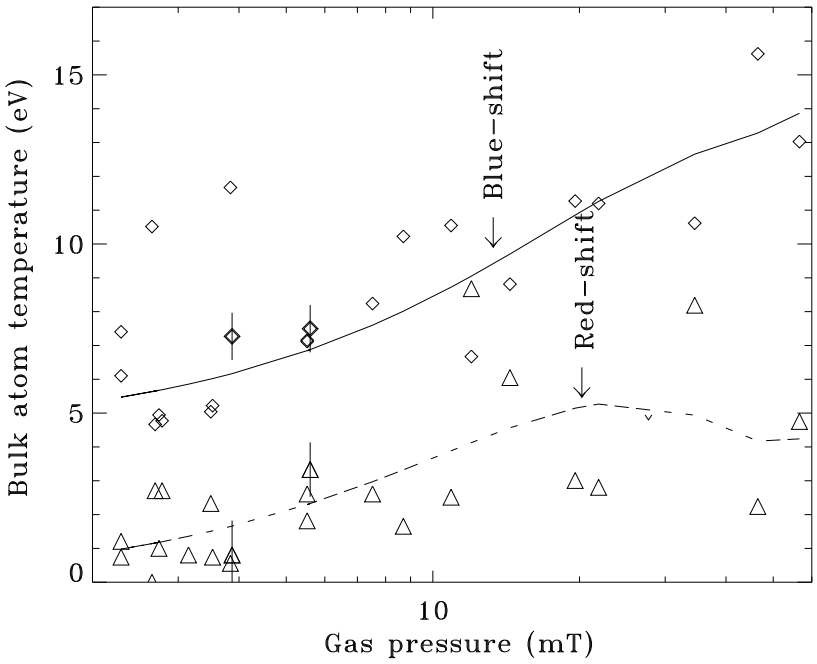
Bulk atom temperature (eV)
15
10
5
0
Blue−shift
Red−shift
10
Gas pressure (mT)

FIG. 9.

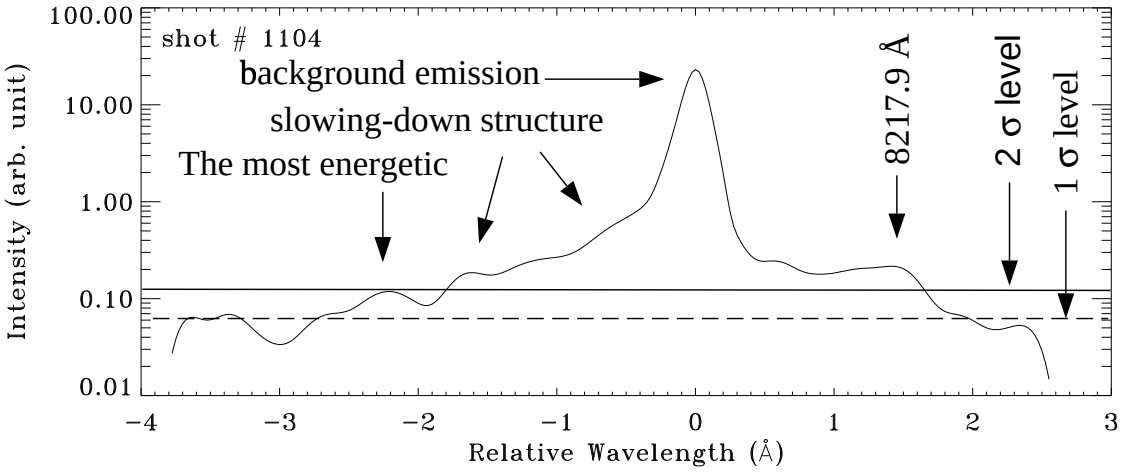
shot # 1104
background emission
slowing-down structure
The most energetic
8217.9 Å
2 σ level
1 σ level
Intensity (arb. unit)
Relative Wavelength (Å)
100.00
10.00
1.00
0.10
0.01
−4
−3
−2
−1
0
1
2
3

FIG. 10.

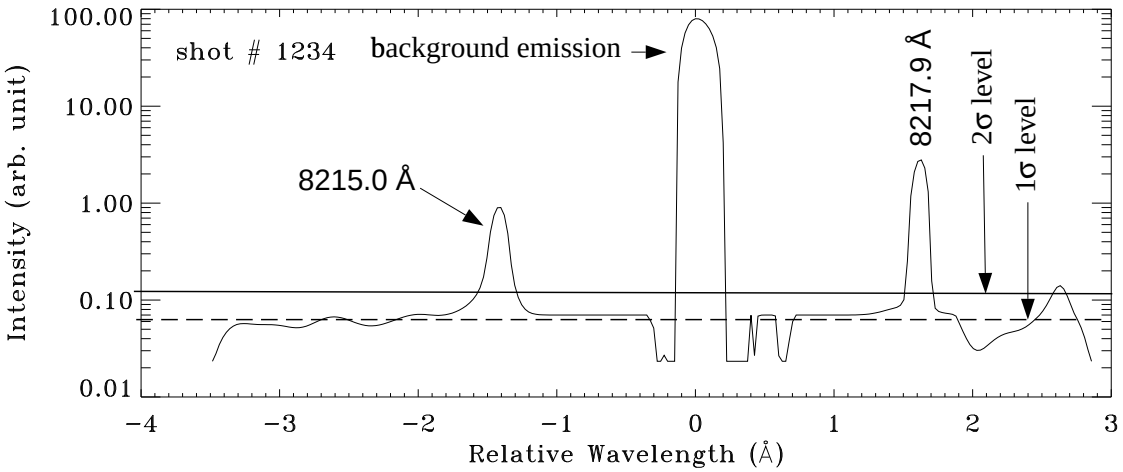
shot # 1234
background emission
8215.0 Å
8217.9 Å
2σ level
1σ level
Intensity (arb. unit)
Relative Wavelength (Å)
100.00
10.00
1.00
0.10
0.01
−4
−3
−2
−1
0
1
2
3

FIG. 11.

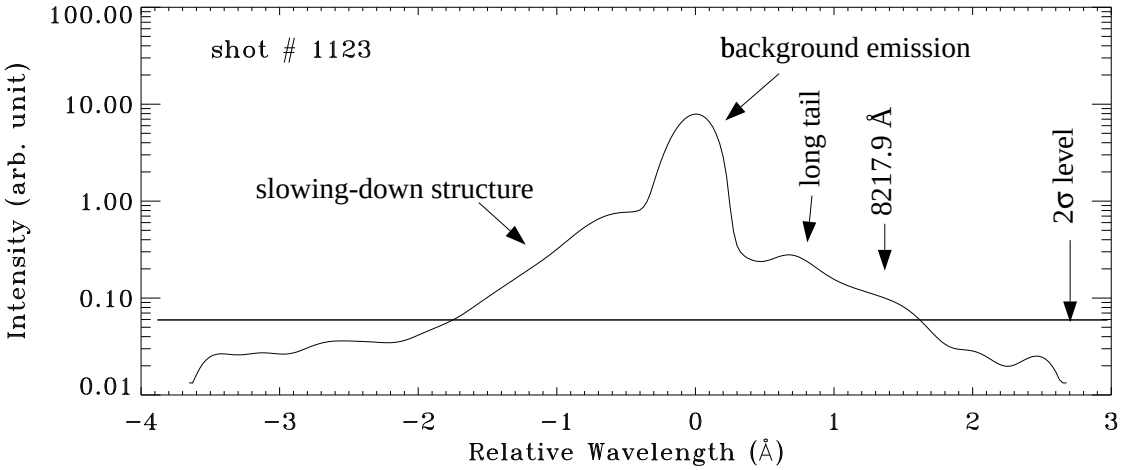
shot # 1123
background emission
long tail
8217.9 Å
2σ level
slowing-down structure
Intensity (arb. unit)
Relative Wavelength (Å)
100.00
10.00
1.00
0.10
0.01
−4
−3
−2
−1
0
1
2
3

FIG. 12.

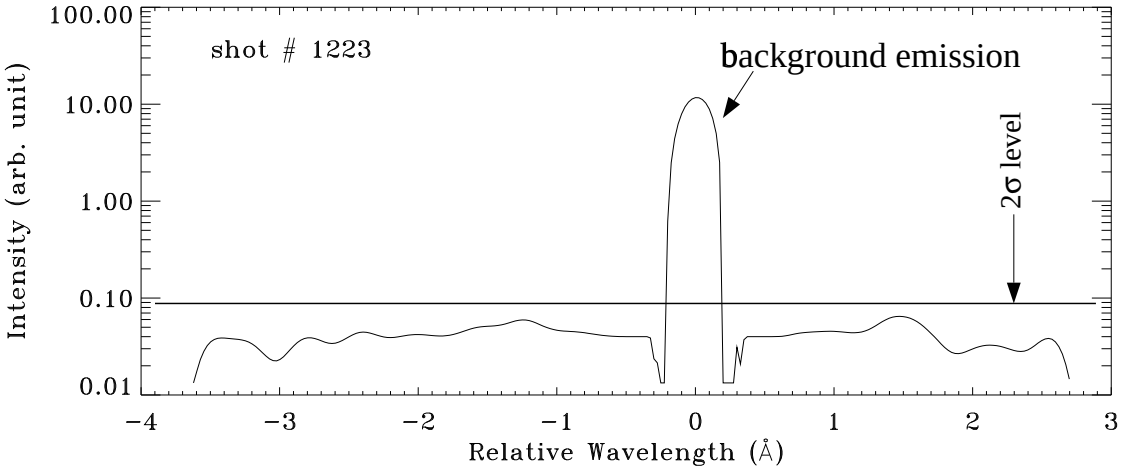
shot # 1223
background emission
2σ level
Intensity (arb. unit)
100.00
10.00
1.00
0.10
0.01
−4
−3
−2
−1
0
1
2
3
Relative Wavelength (Å)

FIG. 13.

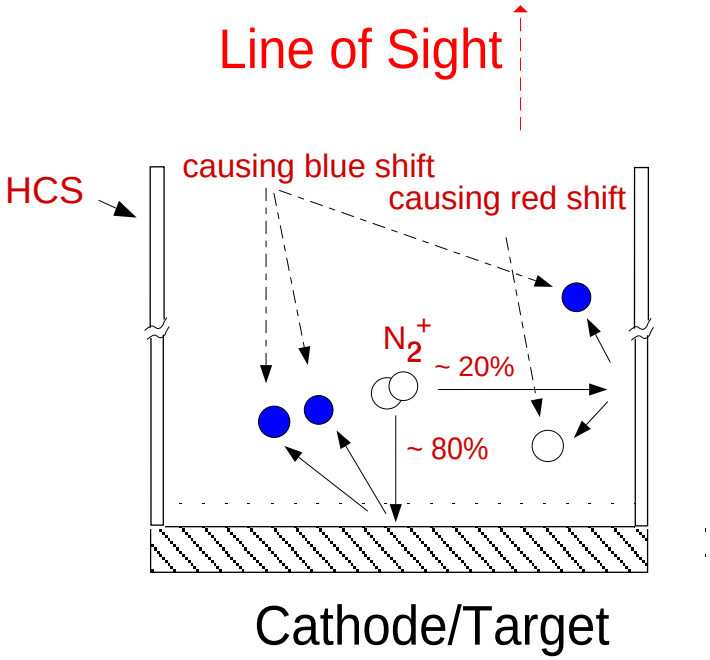
Line of Sight
HCS
causing blue shift
causing red shift
N_2^+
~ 20%
~ 80%
Cathode/Target

FIG. 14.

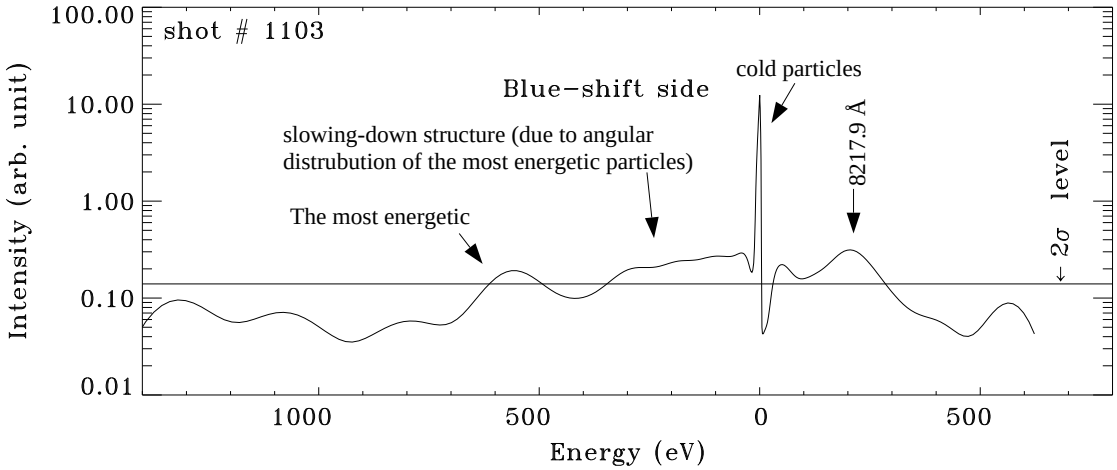
shot # 1103
Blue−shift side
cold particles
8217.9 Å
slowing-down structure (due to angular
distrubution of the most energetic particles)
The most energetic
2σ level
Intensity (arb. unit)
100.00
10.00
1.00
0.10
0.01
1000
500
0
500
Energy (eV)

FIG. 15.

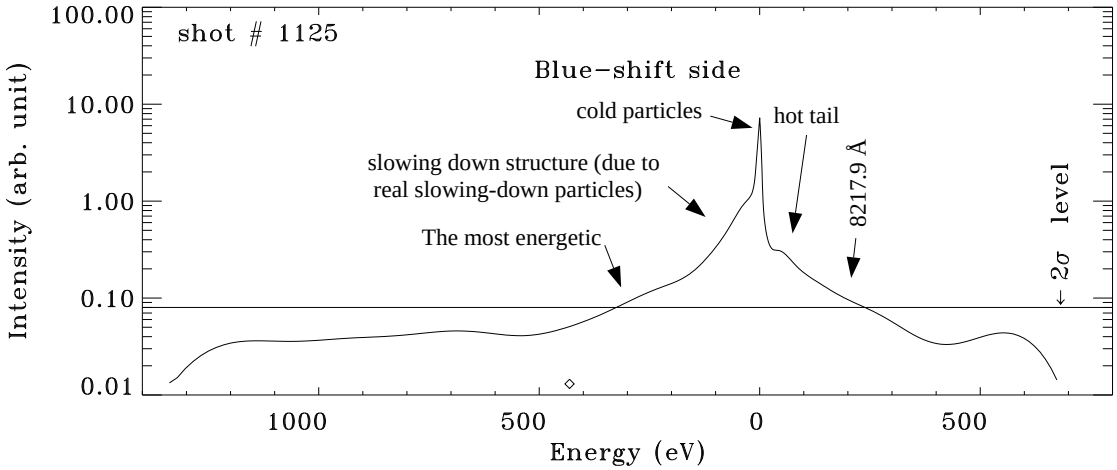
shot # 1125
Blue−shift side
cold particles
hot tail
slowing down structure (due to
real slowing-down particles)
The most energetic
8217.9 Å
2σ level
Intensity (arb. unit)
100.00
10.00
1.00
0.10
0.01
1000
500
0
500
Energy (eV)

FIG. 16.

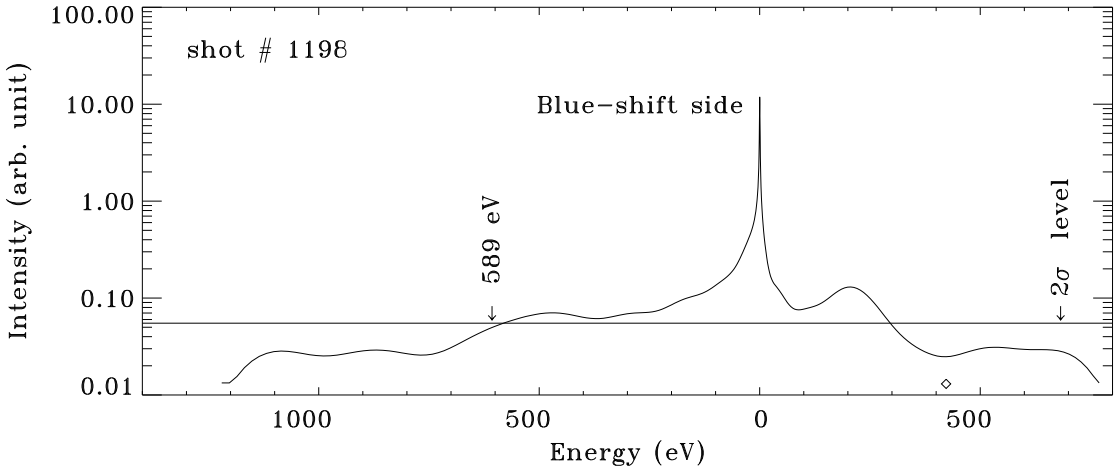
shot # 1198
Blue−shift side
589 eV
2σ level
Intensity (arb. unit)
Energy (eV)
100.00
10.00
1.00
0.10
0.01
1000
500
0
500

FIG. 17.

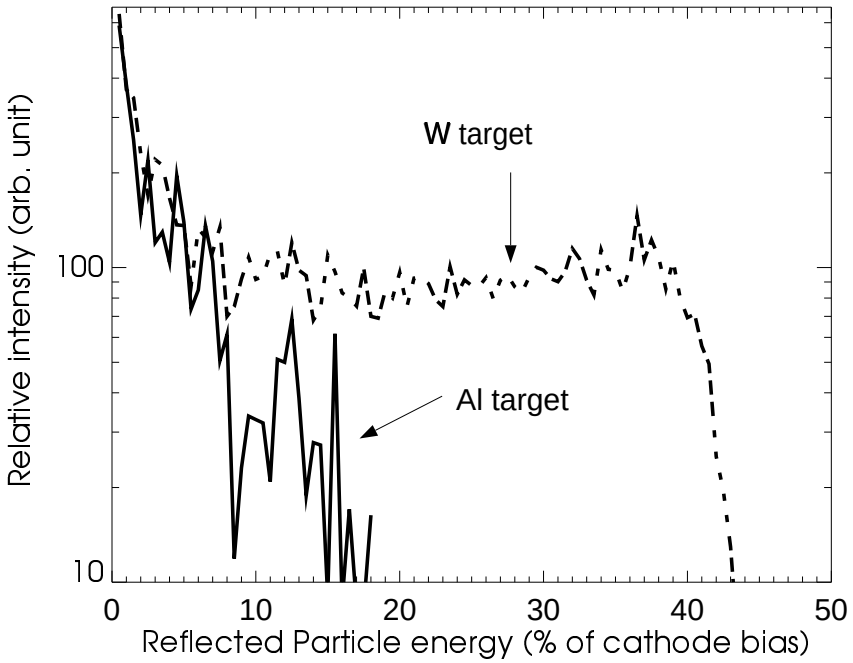
W target
Al target
Relative intensity (arb. unit)
100
10
0
10
20
30
40
50
Reflected Particle energy (% of cathode bias)

FIG. 18.

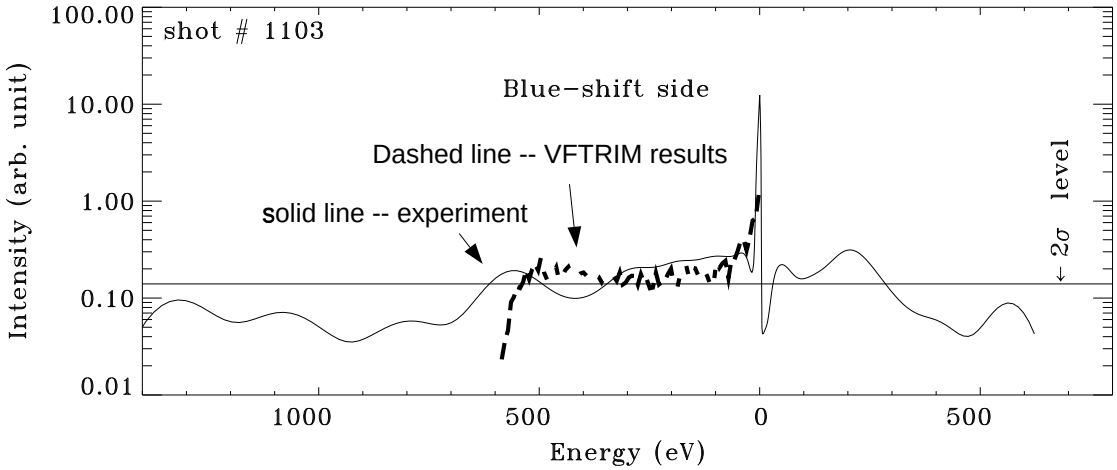
shot # 1103
Blue−shift side
Dashed line -- VFTRIM results
solid line -- experiment
← 2σ level
Intensity (arb. unit)
100.00
10.00
1.00
0.10
0.01
1000
500
0
500
Energy (eV)

FIG. 19.

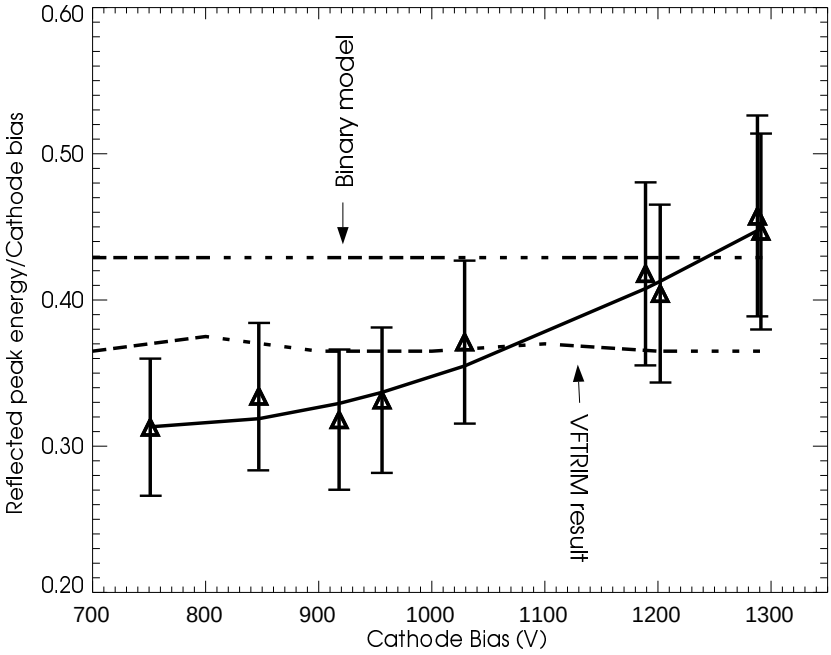
0.60
0.50
0.40
0.30
0.20
Reflected peak energy/Cathode bias
Binary model
VFTRIM result
700
800
900
1000
1100
1200
1300
Cathode Bias (V)